# Structural Diversity within the Mononuclear and Binuclear Active Sites of *N*-Acetyl-D-glucosamine-6-phosphate Deacetylase[†,‡]

Richard S. Hall,[§] Shoshana Brown,[∥] Alexander A. Fedorov,[⊥] Elena V. Fedorov,[⊥] Chengfu Xu,[§] Patricia C. Babbitt,*[,∥] Steven C. Almo,*[,⊥] and Frank M. Raushel*[,§]

*Department of Chemistry, P.O. Box 30012, Texas A&M University, College Station, Texas 77842-3012, Departments of Biopharmaceutical Sciences and Pharmaceutical Chemistry, 1700 4th Street, University of California—San Francisco, San Francisco, California 94158-2550, and Albert Einstein College of Medicine, 1300 Morris Park Avenue, Bronx, New York 10461*

*Received March 20, 2007*

ABSTRACT: NagA catalyzes the hydrolysis of *N*-acetyl-D-glucosamine-6-phosphate to D-glucosamine-6-phosphate and acetate. X-ray crystal structures of NagA from *Escherichia coli* were determined to establish the number and ligation scheme for the binding of zinc to the active site and to elucidate the molecular interactions between the protein and substrate. The three-dimensional structures of the apo-NagA, Zn-NagA, and the D273N mutant enzyme in the presence of a tight-binding *N*-methylhydroxyphosphinyl-D-glucosamine-6-phosphate inhibitor were determined. The structure of the Zn-NagA confirms that this enzyme binds a single divalent cation at the beta-position in the active site via ligation to Glu-131, His-195, and His-216. A water molecule completes the ligation shell, which is also in position to be hydrogen bonded to Asp-273. In the structure of NagA bound to the tight binding inhibitor that mimics the tetrahedral intermediate, the methyl phosphonate moiety has displaced the hydrolytic water molecule and is directly coordinated to the zinc within the active site. The side chain of Asp-273 is positioned to activate the hydrolytic water molecule via general base catalysis and to deliver this proton to the amino group upon cleavage of the amide bond of the substrate. His-143 is positioned to help polarize the carbonyl group of the substrate in conjunction with Lewis acid catalysis by the bound zinc. The inhibitor is bound in the α-configuration at the anomeric carbon through a hydrogen bonding interaction of the hydroxyl group at C-1 with the side chain of His-251. The phosphate group of the inhibitor attached to the hydroxyl at C-6 is ion paired with Arg-227 from the adjacent subunit. NagA from *Thermotoga maritima* was shown to require a single divalent cation for full catalytic activity.

NagA[1] (E.C. 3.5.1.25) is a metal-dependent enzyme which catalyzes the deacetylation of *N*-acetyl-D-glucosamine-6-phosphate to form acetate and D-glucosamine-6-phosphate as presented in Scheme 1. NagA thus catalyzes a key step in the catabolism of *N*-acetyl-D-glucosamine from chitobiose and the recycling of cell wall murein (*1*−*4*). Over 300 sequences homologous to that of NagA from *Escherichia coli* K-12 have been identified in the current NCBI databases. Nearly all of these sequences are annotated as NagA, but some of them are annotated as *N*-acetyl-D-galactosamine-6-phosphate deacetylase (AgaA). In the genome of *E. coli* K-12 there is a deletion which eliminates the genes encoding for the *N*-acetyl-D-galactosamine (Aga) and D-galactosamine (GalN) phosphotransferase systems, while truncating the gene for AgaA. These deletions prevent the growth of *E. coli* K-12 on either *N*-acetyl-D-galactosamine or D-galactosamine (*5*).

Scheme 1

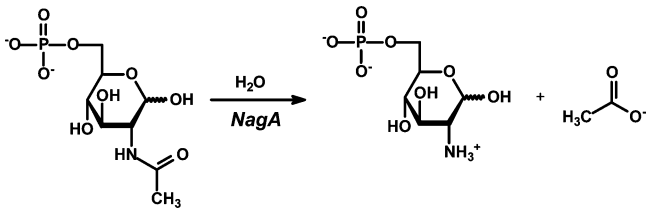


NagA has been characterized as a member of the amidohydrolase superfamily (AHS) based on sequence and structural similarities to other enzymes within this superfamily (*6*). All proteins of the amidohydrolase superfamily possess a $(\beta/\alpha)_8$-barrel structural fold (*7*). The enzymes in this superfamily have been shown to contain $\alpha\beta$-binuclear metal centers (*8*−*13*), α-mononuclear metal centers (*14*−*16*), $\beta$-mononuclear metal centers (*6*, *13*), or metal-independent active sites (*17*).

X-ray crystal structures have been reported for NagA from *Bacillus subtilis* (PDB code: 1un7 (*11*)), *Thermotoga mar-*

[†] This work was supported in part by the NIH (GM71790). R.S.H. was supported by a fellowship from the Chemical Biology Training Grant to Texas A&M University (GM 008523).

[‡] The X-ray coordinates and structure factors for the apo-NagA, Zn-NagA, and the D273N mutant complexed with a transition state inhibitor have been deposited in the Protein Data Bank (PDB accession codes 1ymy, 2p50, and 2p53, respectively).

* To whom correspondence may be addressed. F.M.R.: tel, (979) 845-3373; fax, (979)-845-9452; e-mail, raushel@tamu.edu. P.C.B.: tel, (415) 476-3784; fax, (415)-514-4797; e-mail, babbitt@cgl.ucsf.edu. S.C.A.: tel, (718)430-2746; fax, (718)-430-8565; e-mail, almo@aecom.yu.edu.

[§] Texas A&M University.

[∥] University of California—San Francisco.

[⊥] Albert Einstein College of Medicine.

[1] Abbreviations: *N*-acetyl-D-glucosamine-6-phosphate deacetylase, NagA; *N*-acetyl-D-galactosamine-6-phosphate deacetylase, AgaA; amidohydrolase superfamily, AHS.

10.1021/bi700544c CCC: $37.00 
Published on Web 06/13/2007

*itima* (PDB code: 1o12), and the metal-free complex of *E. coli* (PDB code: 1ymy and 1yrr (*18*)). A comparison of these three X-ray crystal structures of NagA highlights the fundamentally different active site motifs for the complexation of divalent metal ions within this enzyme. The enzyme from *B. subtilis* has an $\alpha\beta$-binuclear metal center with two iron atoms in the active site. The more solvent shielded metal ($M_\alpha$) is coordinated to two histidine residues from $\beta$-strand 1 and an aspartate from $\beta$-strand 8 while the more solvent exposed metal ($M_\beta$) is coordinated to two histidine residues from $\beta$-strands 5 and 6. The two metal ions are bridged to one another by a glutamate from $\beta$-strand 3 and hydroxide or water from solvent (*11*). In contrast, the structure of NagA from *T. maritima* shows only a single iron bound to the $M_\beta$-site and a vacant $M_\alpha$-site. However, the two histidines from $\beta$-strand 1 and the aspartate from $\beta$-strand 8 are apparently available for binding of a second metal ion. The two previously reported structures of NagA from *E. coli* were solved in the absence of any divalent cations, but it is highly probable that NagA from *E. coli* can bind only a single divalent cation at the $M_\beta$-site since the two histidines from $\beta$-strand 1, that are apparently essential for the binding of metal to this site, are absent and replaced by relatively poor metal ligands, asparagine and glutamine.

It is therefore uncertain whether the active sites in NagA from *E. coli* and/or *T. maritima* require one or two metal ions to be fully active. If NagA from either of these organisms has a different requirement for the total number of metal ions required for catalytic activity than NagA from *B. subtilis*, then the chemical mechanism for substrate hydrolysis must also differ in significant ways. The sites for the binding of metal ions in NagA are similar to the other binuclear metal centers found in the amidohydrolase superfamily (*9*, *10*, *13*, *19*). However, in all of these other structures the histidine from $\beta$-strand 5 that coordinates $M_\beta$ interacts with the metal via $N^\delta$, whereas $M_\beta$ in NagA coordinates to $N^\epsilon$. The structures of the metal centers in the active sites of NagA from *B. subtilis*, *T. maritima*, and *E. coli* are presented in Figure 1.

The structure of the wild-type NagA from *E. coli* has now been solved, and we demonstrate that this enzyme binds but a single divalent cation exclusively to the $M_\beta$-site. In addition, the structure of the D273N mutant has been determined in the presence of a transition state inhibitor, and this structure unveils the molecular interactions between the substrate and the enzyme within the active site. An extensive bioinformatics analysis of the sequences annotated as NagA has shown that there is a correlation between the number of metal ions bound in the active site of this enzyme and the presence of a histidine or glutamine at the structural position that is equivalent to His-143 of the enzyme from *E. coli*. This residue is now postulated to facilitate the formation of the tetrahedral intermediate in the mechanism for amide bond cleavage in the active site of NagA.

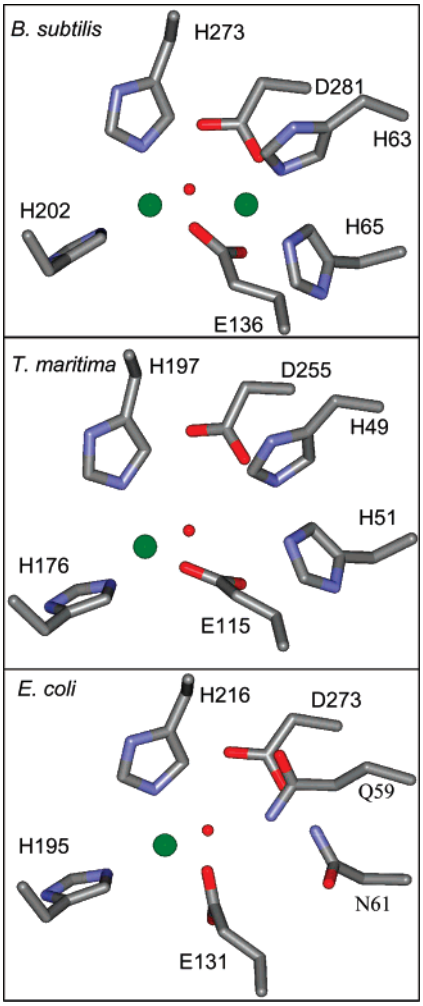


FIGURE 1: Top: The active site of NagA from *B. subtilis* with two Fe ions and a bridging water or hydroxide bound between the two metal atoms (PDB: 1un7). Middle: The active site of NagA from *T. maritima* with one Fe ion and a water molecule (PDB: 1o12). Bottom: The active site of NagA from *E. coli* with one Zn ion and a water molecule (PDB: 2p50). In these images the metal ions are represented as green spheres and the bound water or hydroxide is shown as a smaller red sphere.

## MATERIALS AND METHODS

*Materials.* *N*-Acetyl-D-glucosamine-6-phosphate and purification reagents were purchased from Sigma-Aldrich. Chromatographic columns and resins were purchased from G. E. Healthcare. Chelex 100 resin was purchased from BioRad. Slide-A-Lyzer dialysis cassettes were purchased from Pierce. ICP standards were obtained from Inorganic Ventures Inc. The *N*-methyl phosphonate derivative of D-glucosamine-6-phosphate (**I**) was prepared according to the procedure of Xu (*20*).

*Cloning, Expression, and Purification of NagA.* The wild type NagA and the D273N mutant from *E. coli* K-12 were purified as previously described (*21*). The enzyme utilized for the crystal structure of apo-NagA was expressed in LB growth medium with no additional metal. The NagA gene from *T. maritima* was amplified from genomic DNA using the nucleotide primers 5′-GCAGGAGCCATATGATTGTTGAGAAAGTTCTGATCGTTGATCCCATCG-3′ and 5′-CGCGGAATTCATCTGGATCGAAAAACTACCTCACCC-3′. The product was gel purified and ligated through *Nde*I and *EcoR*I cloning sites into a pET-30a(+) vector incorporating kanamycin resistance and IPTG inducible overexpression. Plasmid DNA was electroporated into XL1 Blue cells and subsequently purified with a Wizard Plus SV miniprep DNA purification system. Gene sequences of the purified plasmids were verified through PCR-based sequencing in

conjunction with the Gene Technologies Laboratory of Texas A&M University.

The NagA from *T. maritima* was expressed in LB medium supplemented with 0.5 mM $ZnCl_2$. The IPTG-induced cells grew for approximately 18 h at 30 °C, after which they were centrifuged at 3400*g* for 12 min. The cells were resuspended in buffer A (50 mM Tris, pH 7.5 and 1.0 mM DTT) which was supplemented with 100 $\mu$g/mL phenylmethanesulfonyl fluoride and disrupted by sonication. Insoluble cell debris was removed by centrifugation at 13900*g* for 12 min, after which 1% w/v protamine sulfate was used to precipitate nucleic acids. The insoluble material was removed by centrifugation. The NagA from *T. maritima* was precipitated between 50 and 75% saturated ammonium sulfate. The precipitated protein was centrifuged at 13900*g* for 12 min. The protein was resuspended in a minimal volume of buffer A and loaded onto a Hiload 26/60 Superdex 200 prep grade gel filtration column. The NagA containing fractions were further purified with a Resource Q anion exchange column via elution with a linear gradient of 1.0 M NaCl in buffer A. Throughout the purification, the NagA containing fractions were identified and monitored for purity by activity analysis and with SDS PAGE. Protein concentrations of NagA from *E. coli* and *T. maritima* were determined using the calculated extinction coefficients of 18490 $M^{-1}$ $cm^{-1}$ and 7680 $M^{-1}$ $cm^{-1}$, respectively (Protein Calculator v3.3 at http://www.scripps.edu/~cdputnam/protcalc.html).

*Measurement of Enzymatic Activity.* The rate of hydrolysis of *N*-acetyl-D-glucosamine-6-phosphate was monitored by observing the cleavage of the amide bond at 215 nm using an extinction coefficient of 254 $M^{-1}$ $cm^{-1}$. Kinetic assays were performed at 30 °C using a 96-well quartz plate with a SpectraMax 384-Plus spectrophotometer from Molecular Devices.

*Reconstitution of NagA from T. maritima.* The metal content (Cd, Co, Cu, Fe, Mn, Ni, and Zn) in the enzyme preparations was determined with ICP-MS. Metal-free NagA from *T. maritima* was prepared via dialysis of a 2.4 mg/mL enzyme solution against 10 mM dipicolinate, 30 mM MES buffer at pH 6.0 using a 10K molecular weight cutoff dialysis cassette with three buffer changes over 3 days. The dipicolinate was removed with four buffer changes against 30 mM metal-free HEPES at pH 8.0. For the metal reconstitution study, aliquots of apoenzyme were incubated with 0 to 3 equiv of $ZnCl_2$ per subunit at 4 °C for 24 h with 50 $\mu$M enzyme. The enzymatic activity of the reconstituted protein was determined after a 5000-fold dilution into a 2.0 mM *N*-acetyl-D-glucosamine-6-phosphate assay mixture containing 50 mM Tris buffer at pH 7.5 and 30 °C.

*Sequence Collection.* NagA-like sequences were found by searching the NCBI protein database via the HMMSEARCH program, using hidden Markov models (HMMs) from the Structure−Function Linkage Database (*22*). The HMMs were based on alignments for the *N*-acetyl-D-glucosamine-6-phosphate deacetylase family, the *N*-acetyl-D-galactosamine-6-phosphate deacetylase family, and the *N*-acetyl-D-glucosamine-6-phosphate deacetylase/*N*-acetyl-D-galactosamine-6-phosphate deacetylase-like subgroup. All sequences were then aligned to the *N*-acetyl-D-glucosamine-6-phosphate deacetylase/*N*-acetyl-D-galactosamine-6-phosphate deacetylase-like subgroup HMM via the HMMALIGN program and examined for conservation of subgroup-specific catalytic residues. Sequences that appeared to be fragments or did not conserve all subgroup-specific catalytic residues were removed from the sequence set.

Table 1: Data Collection and Refinement Statistics

| crystal | SeMet• apo-NagA | WT NagA•Zn | D273N NagA• Zn•TS-inhibitor |
|---|---|---|---|
| | Data Collection | | |
| beamline | NSLS X29 | NSLS X4A | NSLS X4A |
| wavelength (Å) | 0.9783 peak | 0.979 | 0.979 |
| space group | $P2_12_12$ | $C222_1$ | $P3_121$ |
| mol. in au | 2 | 4 | 2 |
| unit cell parameters | | | |
| *a* (Å) | 82.23 | 95.18 | 81.40 |
| *b* (Å) | 114.02 | 117.99 | 81.40 |
| *c* (Å) | 80.22 | 265.60 | 206.45 |
| resolution (Å) | 2.6 | 2.2 | 2.1 |
| unique reflections | 23035 | 72816 | 45044 |
| completeness (%) | 96.8 | 95.9 | 95.4 |
| $R_{merge}$ | 0.079 | 0.082 | 0.086 |
| average $I/\sigma$ | 23.6 | 19.1 | 19.7 |
| | Refinement | | |
| resolution (Å) | 25.0−2.6 | 25.0−2.2 | 25.0−2.1 |
| $R_{cryst}$ | 0.212 | 0.213 | 0.205 |
| $R_{free}$ | 0.243 | 0.257 | 0.242 |
| rmsd, bonds (Å) | 0.008 | 0.006 | 0.006 |
| rmsd, angles (deg) | 1.4 | 1.3 | 1.2 |
| protein atoms | 5306 | 10854 | 5748 |
| waters | 0 | 351 | 326 |
| $Zn^{+2}$ | 0 | 4 | 2 |
| inhibitor atoms | 0 | 0 | 40 |
| PDB ID | 1YMY | 2P50 | 2P53 |

*Cytoscape.* A custom database was created, containing the NagA-like sequences. BLAST searches were then performed against the database at an *e*-value cutoff of $1 \times 10^{-57}$, using each sequence in the set as a query. A cytoscape network was created based on the BLAST results, where each node represents a single sequence in the NagA-like sequence set and each edge represents the most significant BLAST *e*-value connecting the two sequences. The nodes are arranged using organic layout. The amino acid types present at positions corresponding to the first two metal binding ligands in the *B. subtilis* NagA and His-143 in the *E. coli* NagA were determined based on the alignment described in the following section.

*Sequence Alignment.* All sequences in the NagA-like sequence set were aligned using Muscle (*23*). The alignment was hand edited to ensure that catalytic residues were correctly aligned and to remove unaligned regions at the N- and C-termini, and is available in the Supporting Information.

*Bayesian Phylogenetic Tree.* A representative subset of NagA-like sequences was selected by filtering the entire NagA-like sequence set to approximately 40% identity using the mcd-hit program (*24*). A filtered version of the hand-edited alignment described in the previous section, containing only those sequences in the 40% identity filtered set, was then created and used for tree construction with MrBayes (*25*).

*Crystallization and Data Collection.* Three different crystal forms (Table 1) were grown by the hanging drop method at room temperature: selenomethionine (SeMet)-substituted apo-NagA; wild type NagA and $Zn^{+2}$; and D273N NagA mutant, $Zn^{+2}$ with the transition state inhibitor *N*-methylhydroxyphosphinyl-D-glucosamine-6-phosphate (**I**). The crystallization conditions utilized the following conditions:

(1) SeMet-substituted apo-NagA. The protein solution contained SeMet-substituted NagA from *E. coli* (12 mg/mL), 20 mM HEPES, pH 7.5, and 5 mM mercaptoethanol; the precipitant contained 1.6 M ammonium sulfate, 0.1 M Tris HCl, pH 8.5. Crystals appeared in 3 days and exhibited diffraction consistent with the space group $P2_12_12$ with two molecules of NagA per asymmetric unit.

(2) NagA and $Zn^{2+}$. The protein solution contained wild type NagA (15 mg/mL), 20 mM HEPES, pH 7.5; the precipitant contained 25% PEG 3350, 0.1 M Tris HCl, pH 8.5, and 0.2 M $ZnCl_2$. Crystals appeared in 6 days and exhibited diffraction consistent with the space group $C222_1$, with four molecules of NagA per asymmetric unit.

(3) NagA D273N, $Zn^{2+}$, and transition state inhibitor, *N*-methylhydroxyphosphinyl-D-glucosamine-6-phosphate (**I**). The protein solution contained NagA mutant D273N (20 mg/mL), 20 mM HEPES, pH 7.5, 1 mM $ZnCl_2$, and 40 mM inhibitor; the precipitant contained 12% PEG 3350, 0.1 M Hepes, pH 7.5, and 1 mM $ZnCl_2$. Crystals appeared in 1 week and exhibited diffraction consistent with the space group $P3_121$ with two molecules of NagA per asymmetric unit.

Prior to data collection, the crystals were transferred to cryoprotectant solutions composed of their mother liquids and 20% glycerol. After ~10 s incubation, the crystals were flash-cooled in a nitrogen stream. A single-wavelength anomalous dispersion (SAD) data set for a crystal of SeMet-substituted apo-NAgA (Table 1, column 1) was collected to 2.6 Å resolution at the NSLS X29 beamline (Brookhaven National Laboratory) on an ADSC Q315 detector. Data sets for the wild type NagA complex with $Zn^{2+}$ (column 2), and D273N NagA complex with $Zn^{2+}$ and *N*-methylhydroxyphosphinyl-D-glucosamine-6-phosphate (column 3) were collected at the NSLS X4A beamline on an ADSC CCD detector to 2.2 Å and 2.1 Å, respectively. Diffraction intensities were integrated and scaled with programs DENZO and SCALEPACK (*26*). The data collection statistics are given in Table 1.

*Structure Determination and Refinement.* Initial attempts to determine the structure of the apo-NagA by molecular replacement using the structures of the NagA from *B. subtilis* (PDB ID 1un7) and NagA from *T. maritima* (PDB ID 1o12) as search models were unsuccessful. Instead, the structure of the SeMet-substituted apo-NagA was solved by SAD with the program SOLVE (*27*); fourteen of the sixteen selenium sites were identified. These heavy atom sites were used to calculate initial phases, which were improved by solvent flattening and NCS averaging with the program RESOLVE (*28*), yielding an interpretable map for two monomers in the asymmetric unit for space group $P2_12_12$. Iterative cycles of manual rebuilding with TOM (*29*) and refinement with CNS (*30*) resulted in a model at 2.6 Å resolution with $R_{cryst} = 0.212$ and $R_{free} = 0.243$. The two polypeptides (residues 1−382 each) in the asymmetric unit were assembled as a dimer. The chain segment 139−144 of the monomer A and chain segments 69−73, 138−152, and 277−307 of the monomer B were missing in the electron density maps. The active sites of both monomers did not contain $Zn^{2+}$.

The structure of the wild type NagA crystallized with $Zn^{2+}$ was solved by molecular replacement with the program PHASER (*31*), using the SeMet substituted apo-NagA structure as the search model. Iterative cycles of automatic rebuilding with ARP (*32*), manual rebuilding with TOM, and refinement with CNS were performed. The model was refined at 2.2 Å with $R_{cryst} = 0.213$ and $R_{free} = 0.257$. The four polypeptides (residues 1−382 each) in the asymmetric unit were assembled as two dimers. The chain segment 280−307 in three out of four monomers was missing in the electron density maps. A $Zn^{2+}$ was clearly visible in the electron density maps for all four monomers.

The structure of the D273N NagA mutant crystallized with $Zn^{2+}$ and *N*-methylhydroxyphosphinyl-D-glucosamine-6-phosphate (**I**) was also solved by molecular replacement using SeMet substituted apo-NagA as the search model. The model was refined at 2.1 Å with $R_{cryst} = 0.205$ and $R_{free} = 0.242$. All residues (1−382) were ordered in both polypeptides. The TS-inhibitor and $Zn^{2+}$ were also well-defined in both polypeptides of the asymmetric unit.

## RESULTS

*Bioinformatics.* Approximately 350 NagA-like sequences in the NCBI protein database were identified. The majority of these sequences (89%) are found in bacteria, reflecting their roles in cell wall peptidoglycan and teichoic acid biosynthesis in these organisms. Ten percent of the sequences are found in eukaryotes, and the remaining 1% are found in archaea. The AgaA protein sequence from *E. coli* C was compared to similar sequences in the NCBI database. Only six distinct sequences are annotated as AgaA. All of these proteins possess about a 30% sequence identity with NagA from *E. coli* K-12. All of the AgaA enzymes are found in different strains of *E. coli* except for one example. The AgaA from *T. elongatus* BP-1 was located next to D-glucosamine-related enzymes. Several of the organisms, including *E. coli* HS and *E. coli* 101-1, contain two sequences annotated as NagA with less than 30% sequence identity. Many of the NagA annotated enzymes that are closely related to the sequence of AgaA, like that of *Vibrio vulnificus* and *Aeromonas hydrophilla,* are located in the chromosome next to genes that are expected to operate on D-galactosamine such as *N*-acetyl-D-galactosamine phosphotransferase components, tagatose-1,6-bisphosphate aldolase, tagatose-6-phosphate kinase, and α-galactosidase. Careful analysis of the sequence alignment of NagA and AgaA enzymes indicates that AgaA contains all of the important catalytic residues required for NagA. A small, representative alignment of the three NagA enzymes discussed here with AgaA from *E. coli* C is shown in Figure 2.

*Metal Dependence and Activity of NagA from T. maritima.* The recombinant NagA from *T. maritima* was purified from an *E. coli* expression system and found to contain 0.25 equiv of Zn and 0.35 equiv of Fe per active site. Upon further incubation with 3 molar equiv of Zn, values of $k_{cat}$ and $K_m$ were determined to be $110 \pm 3$ s$^{-1}$ and $0.04 \pm 0.01$ mM, respectively, with a value of $k_{cat}/K_m$ of $2.8 \pm 0.4 \times 10^6$ M$^{-1}$ s$^{-1}$. At high substrate concentrations the activity diminished with an inhibition constant of $3.9 \pm 0.5$ mM. After removal of the bound metal, NagA from *T. maritima* lacked detectable levels of activity. The apoenzyme was reconstituted by adding up to 3 equiv of zinc per subunit. In these experiments there was a linear increase in the catalytic activity that reached a maximum at approximately 1 equiv of zinc per enzyme subunit. The change in activity as a function of added

```
E.c. AgaA   1 MSGRGRNMTHVLRARRLLTEEGWLDDHQLRIADGVIAAIEPIPAG------VTERDAELLCPAYIDTHVHGGAGVDVMDDAPDV----LDK
B.s. NagA   1 -----MAESLLIKDIAIVTENEVIKNGYVGINDGKISTVSTERPKEPYSKEIQAPADSVLLPGMIDIHIHGGYGADTMDASFST----LDI
T.m. NagA   1 ---------MIVEKVLIVDPIDGEFTGDVEIEEGKIVKVEKR----------ECIPRGVLMPGFVDPHIHGVVGADTMNCDFS-------E
E.c. NagA   1 --------MYALTQGRIFTGHEFLDDHAVVIADGLIKSVCPVAELPP-EIEQRSLNGAILSPGFIDVQLNGCGGVQFNDTAEAVSVETLEI

E.c. AgaA  82 LAMHKAREGVGSWLPTTVTTPLNTIHAALKRIAQRCQRGGP---GAQVLGSYLEGPYFTPQNKGAHPPELFRELEIAELDQLIAVSQHTLR
B.s. NagA  83 MSSRLPEEGTTSFLATTITQEHGNISQALVNAREWKAAEESSLLGAELLGIHLEGPFVSPKRAGAQPKEWIRPSDVELFKKWQQEAGGLIK
T.m. NagA  66 MEEFLYSQGVTTFLATTVSTSLEKMKEILRKARDYILENPS----TSLLGVHLEGPYISKEKKGAHSEKHIRPPSERELSEIDSPA----K
E.c. NagA  83 MQKANEKSGCTNYLPTLITTSDELMKQGVRVMREYLAKHPN-----QALGLHLEGPWLNLVKKGTHNPNFVRKPD-AALVDFLCENADVIT

E.c. AgaA 168 VVALAPEKEGALQAIRHLKQQNVKVMLGHRAATWQQTRAAFDACADRLVHCYNRMTGLHHREPGIVCAGLTDKRAWLELIADGHHVHPAAM
B.s. NagA 172 IVTLAPEEDQHFELIRHLKDESIIASMGHTDADSALLSDAAKAGASHMTHLYNAMSPFHHREPGVIGTALAHDGFVTELIADGIHSHPLAA
T.m. NagA 148 MLTFAPEIE-SSELLLRLVKRDIVLSAGHSIATFEEFMKFYKEGVKRITHFPNGLKPLHHREIGITGAGLLLDDVKLELICDGVHLSREMV
E.c. NagA 166 KVTLAPEMVP-AEVISKLANAGIVVSAGHSNATLKEAKAGFRAGITFATHLYNAMPYITGREPGLAGAILDEADIYCGIIADGLHVDYANI

E.c. AgaA 271 SLCCCCAKER-IVLITDAMQAAGMPDGRYTLCGEEVQMHGGVVRTASGGLAGSTLSVDAAVRNMVELTGVTPAEAIHMASLHPARMLGVDG
B.s. NagA 266 KLAFLAKGSSKLILITDSMRAKGLKDGVYEFGGQSVTVRGRTALLSDGTLAGSILKMNEGARHMREFTNCSWTDIANITSENAAKQLGIFD
T.m. NagA 239 KLVYKVKKANGIVLVTDSISAAGLKDGTTTLGDLVVKVKDGVPRLEDGTLAGSTLFFSQAVKNFRKFTGCSITELAKVSSYNSCVELGLDD
E.c. NagA 258 RNAKRLKGDK-LCLVTDATAPAGANIEQFIFAGKTIYYRNGLCVDENGTLSGSSLTMIEGVRNLVEHCGIALDEVLRMATLYPARAIGVEK

E.c. AgaA 351 VLGSLKPGKRASVVALDSGLHVQQIWIQGQLASF------
B.s. NagA 356 RKGSVTVGKDADLVIVSSDCEVILTICRGNIAFISKEADQI
T.m. NagA 330 R-GRIAEGTRADLVLLDEDLNVVMTIKEGEVVFRSR----
E.c. NagA 348 RLGTLAAGKVANLTAFTPDFKITKTIVNGNEVVTQ-----
```

FIGURE 2: Protein sequence alignment of AgaA from *E. coli* C, NagA from *B. subtilis*, NagA from *T. maritima*, and NagA from *E. coli* K-12. The eight $\beta$-strands are highlighted in gray. The residue positions from the end of $\beta$-strand 1 that ligate the $\alpha$-metal ion are highlighted in yellow. The residue position that corresponds to His-143 in NagA from *E. coli* K-12 is highlighted in green. Fully conserved metal binding and catalytic residues are highlighted in red. Fully conserved substrate binding residues are highlighted in blue.

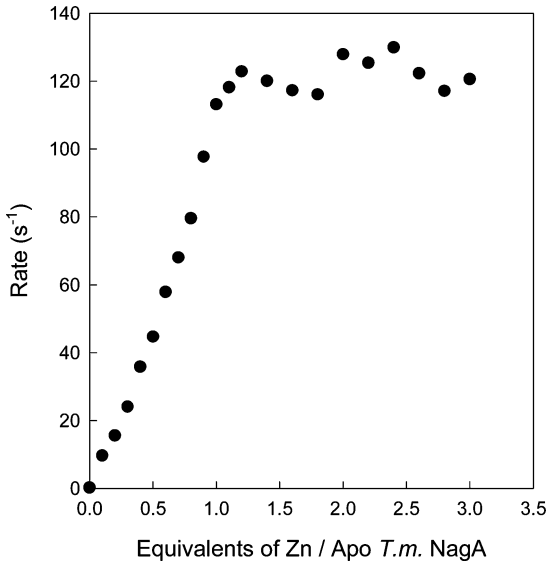


FIGURE 3: Reconstitution of apo-NagA from *T. maritima* (50 $\mu$M) with varying amounts of $ZnCl_2$. The rate of substrate hydrolysis was determined with 2.0 mM *N*-acetyl-D-glucosamine-6-phosphate. Additional details are provided in the text.

zinc is presented in Figure 3. These results demonstrate that NagA from *T. maritima* requires only a single divalent cation for maximum catalytic activity.

*Structure of Apo-NagA.* The crystal structure of the apo-NagA was determined to a resolution of 2.6 Å in the absence of any other ligands. The enzyme adopts a homotetrameric oligomerization state in solution as determined by gel filtration chromatography (*21*), SAXS (*18*) and analytical ultracentrifugation (*33*). The quaternary structure is a dimer of dimers, where each dimer pair has the active sites facing the complementary subunit as presented in Figure 4A. Interactions for this active site interface occur mainly through a loop and $\alpha$-helix region located after $\beta$-strand 6. Arg-227 is poised to interact with the phosphate moiety of the substrate molecule which would bind to the complementary subunit as shown previously for the NagA from *B. subtilis* (*11*). Other interactions between the two dimers occur between the $\beta$-sandwich domains formed by residues from the N- and C-termini. The tertiary fold consists of a somewhat twisted $(\beta/\alpha)_8$-barrel barrel made of eight alternating $\beta$-strands and $\alpha$-helices as shown in Figure 4B. A small $\alpha$-helix partially covers the N-terminus (bottom) of the barrel. The putative active site residues are located at the C-terminal end of the $\beta$-barrel. The loop region between $\beta$-strands 3 and 4, which contains residues 138−145, is conspicuously absent in the structure of the apo-NagA. This is likely due to the mobility of these residues in the absence of a bound ligand. A small $\beta$-sheet formed by residues between $\beta$-strand 8 and $\alpha$-helix 9 forms a putative capping domain near the active site.

*Structure of Zn-NagA.* The structure of the wild type NagA from *E. coli* was determined in the presence of zinc bound within the active site. Each subunit binds a single Zn atom in the $M_\beta$ site, through electrostatic interactions with Glu-131, His-195, and His-216 as shown in Figure 5. The interatomic distances of Zn to these residues in the native structure are 2.1, 2.2, and 2.1 Å, respectively. Subunit A possesses two water molecules in the active site. One of these water molecules is bound directly to the Zn at a distance of 2.5 Å. This water molecule is also interacting with both oxygen atoms of Asp-273 at distances of 2.8 and 3.0 Å. A second active site water molecule is 2.9 Å from the first water molecule and is hydrogen bonded to $\delta$-O of Asn-61 and to one of the oxygen atoms from the carboxylate side chain of Glu-131 with distances of 2.5 and 2.7 Å, respectively. Subunit B also contains two water molecules in the active site with similar distances and geometries.

*Structure of D273N Mutant.* The zinc in the active site of the wild type NagA from *E. coli* is coordinated to a single water molecule, and this water molecule is hydrogen bonded to the side chain carboxylate of Asp-273 from $\beta$-strand 8. Mutation of this residue to asparagine results in a protein that is unable to hydrolyze the substrate (*21*). The crystal structure of the D273N mutant was determined in the presence of a transition state analogue inhibitor (**I**) in an attempt to unveil the molecular interactions between the

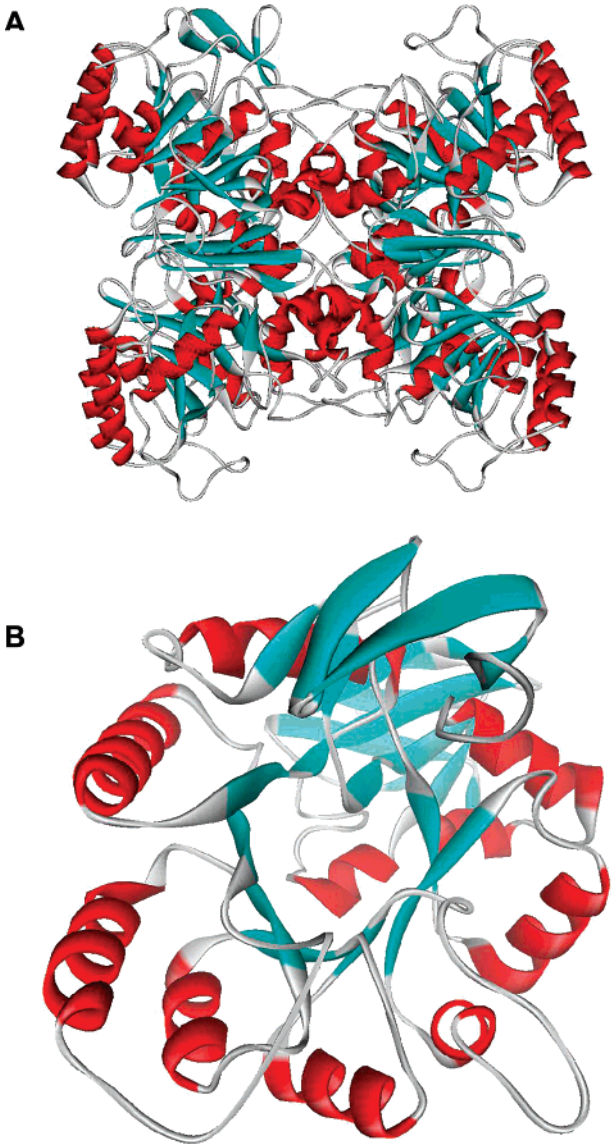


FIGURE 4: Ribbon diagram of the three-dimensional structure of NagA from *E. coli* displaying the tetrameric oligomerization (A). Ribbon diagram of an individual subunit of NagA (B).

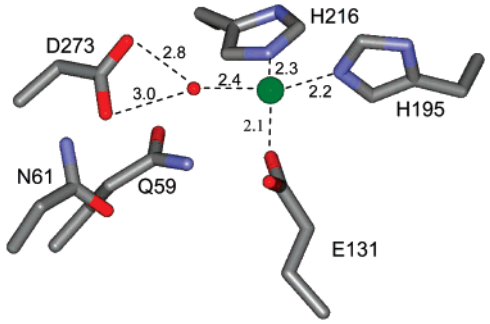


FIGURE 5: The structure of the active site of NagA from *E. coli* showing the coordination of the single Zn in the $\beta$-metal site. The zinc is represented as a green sphere, and the bound water molecule is shown as a small red sphere. The distances between the zinc and the coordinating ligand are listed in angstroms.

protein and substrate in a complex that cannot be hydrolyzed. The inhibitor, *N*-methylhydroxyphosphinyl-D-glucosamine-6-phosphate (**I**), is presented in Scheme 2 and is bound within the active site of D273N. The active site Zn in this structure is coordinated by four ligands in a distorted tetrahedral

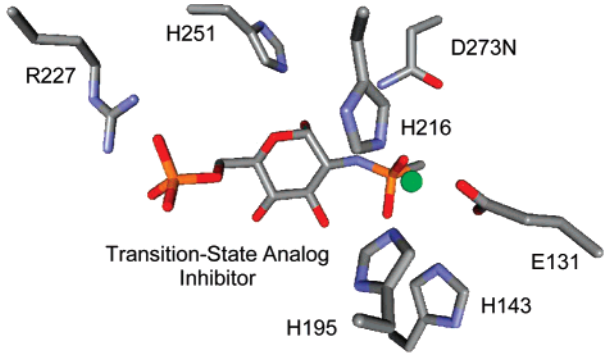


FIGURE 6: The structure of the active site of the NagA mutant D273N in the presence of the tight-binding transition state inhibitor **I**.

Scheme 2

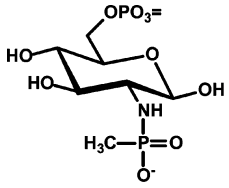


(**I**)

fashion. One of these interactions is from one of the side-chain carboxylate oxygens of Glu-131 from $\beta$-strand 3 at a distance of 1.8 Å. There are additional interactions from His-195 from $\beta$-strand 5 and His-216 from $\beta$-strand 6 at distances of 2.1 and 2.2 Å, respectively. The fourth interaction is from one of the phosphonate oxygens of the inhibitor at a distance of 2.0 Å and is analogous to the water ligand described previously for the wild-type Zn structure. There are two other atoms near the active site Zn at slightly longer distances. These include the other oxygen from the phosphonate moiety of the inhibitor (analogous to the substrate carbonyl) and the second carboxylate oxygen of Glu-131. The oxygen from the inhibitor is positioned 3.0 Å away from the zinc and 3.0 Å from the side chain of His-143. The second carboxylate oxygen of Glu-131 is 2.9 Å away from Zn and 2.9 Å away from His-143. His-251 is hydrogen bonded to the anomeric hydroxyl of the inhibitor in the α-conformation at a distance of 2.7 Å. Two of the phosphate oxygens from the inhibitor are positioned 2.8 and 3.0 Å from the guanidino group of Arg-227, which originates from the adjacent subunit. The X-ray crystal structure of the active site residues with bound Zn and inhibitor ligands is presented in Figure 6. A schematic drawing of the inhibitor−enzyme interactions is presented in Figure 7.

## DISCUSSION

*Differentiation of AgaA and NagA.* The sequence alignment between NagA and those proteins annotated as AgaA demonstrates that all of the important catalytic residues and the amino acids required for substrate recognition are conserved. These results suggest that those proteins currently annotated as NagA in the various databases are also able to hydrolyze the acetyl group from *N*-acetyl-D-galactosamine-6-phosphate. This conjecture has been confirmed for the NagA from *E. coli* K-12 (*21*).

*Biological Functions within the NagA-like Sequence Group.* A Bayesian phylogenetic tree (Figure 8) and sequence-

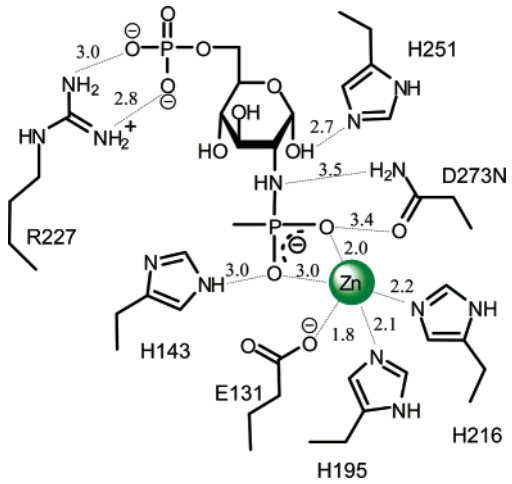


FIGURE 7: A schematic drawing of the active site of the D273N NagA mutant from *E. coli* with the bound transition state analogue inhibitor **I**. The distances between key molecular interactions are listed in angstroms.

similarity based clustering (Figure 9A) separate the NagA-like sequences roughly as would be expected based on species. However, some groups, most strikingly proteobacteria, have more than one sequence cluster. Although many of the NagA-like sequences are likely to function as *N*-acetyl-D-glucosamine-6-phosphate deacetylases (and, indeed, several have been experimentally characterized as such), some may have slightly different substrate specificity. For example, one of the NagA-like sequences from *E. coli* (gi|8895751) has been shown, based on experiment and operon context, to encode an *N*-acetyl-D-galactosamine-6-phosphate deacetylase (AgaA) (*5*). Many strains of *E. coli* have at least two distinct NagA-like sequences, one with a likely primary biological function of NagA and one with a likely primary biological function of AgaA.

Genome context information suggests that AgaA and NagA may not be the only biologically relevant functions found in the NagA-like sequence group. For example, genome context suggests that one of the NagA-like sequences from *Vibrio furnissii* (gi|3122428), which has been shown experimentally to complement an *E. coli* NagA mutant, may actually function as an *N*-acetyl-D-mannosamine-6-phosphate deacetylase *in vivo* (*34*). At least 38 distinct strains (corresponding to 23 species) contain multiple NagA-like sequences that share less than 50% identity to each other, suggesting that one of the sequences may have a slightly altered substrate specificity or expression pattern.

*Differentiation of Mononuclear and Binuclear Forms of NagA.* While *B. subtilis* NagA binds two metals (*11*), *T. maritima* and *E. coli* NagA bind only a single metal. One obvious candidate for the sequence signature responsible for this change is the HxH motif found in *B. subtilis* NagA, but replaced by QxN in *E. coli* NagA, which provides two of the four ligands for the α-metal. Figure 9B shows the NagA-like sequence Cytoscape network, with sequences possessing the HxH motif colored red, sequences possessing the QxN motif colored blue and sequences possessing an intermediate HxN motif colored green. Although none of the sequences

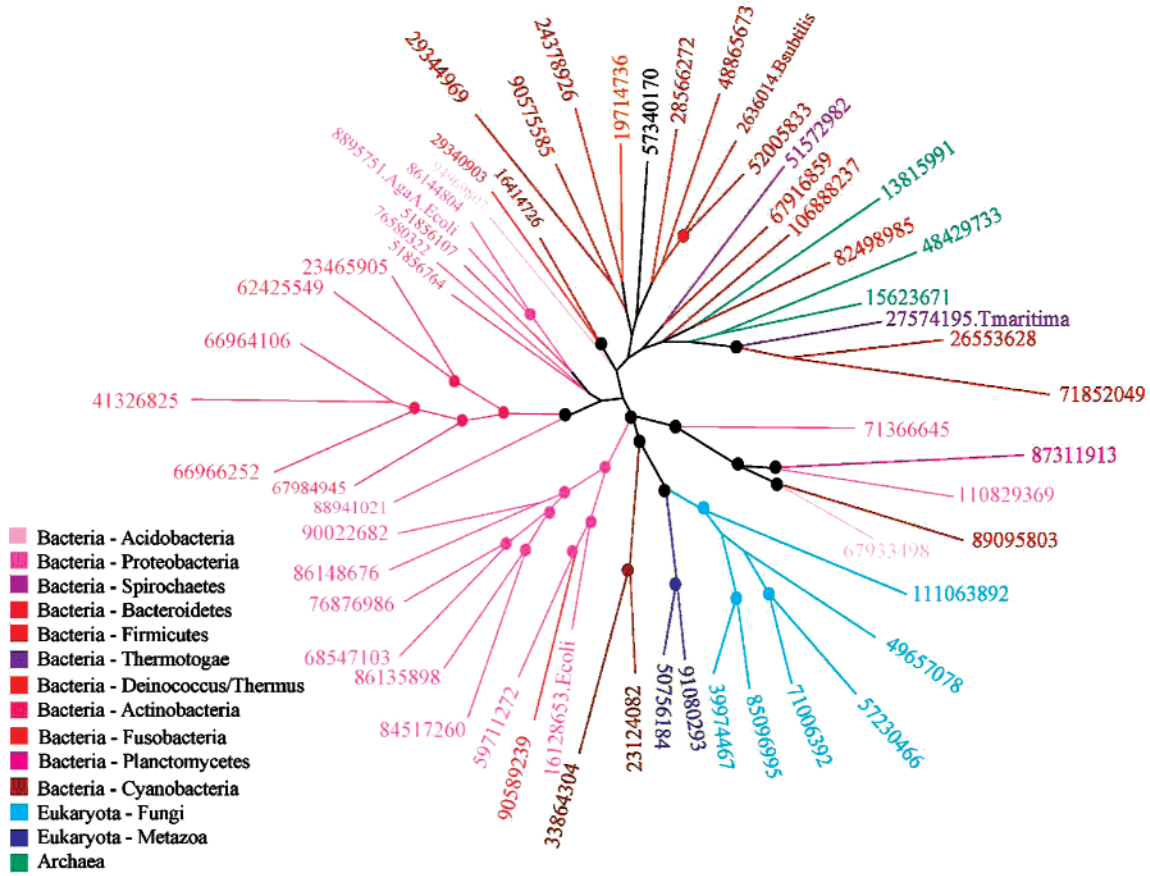


FIGURE 8: Bayesian phylogenetic tree of the proteins in the NagA-like sequence group. A representative set of sequences was selected by filtering the complete NagA-like sequence set to approximately 40% identity. Sequences are listed according to their NCBI gi number. The crystallized NagA sequences from *E. coli*, *B. subtilis*, and *T. maritima* and the experimentally characterized AgaA from *E. coli* are indicated with species abbreviations. Branch confidence values of greater than 0.9 are indicated as circles.

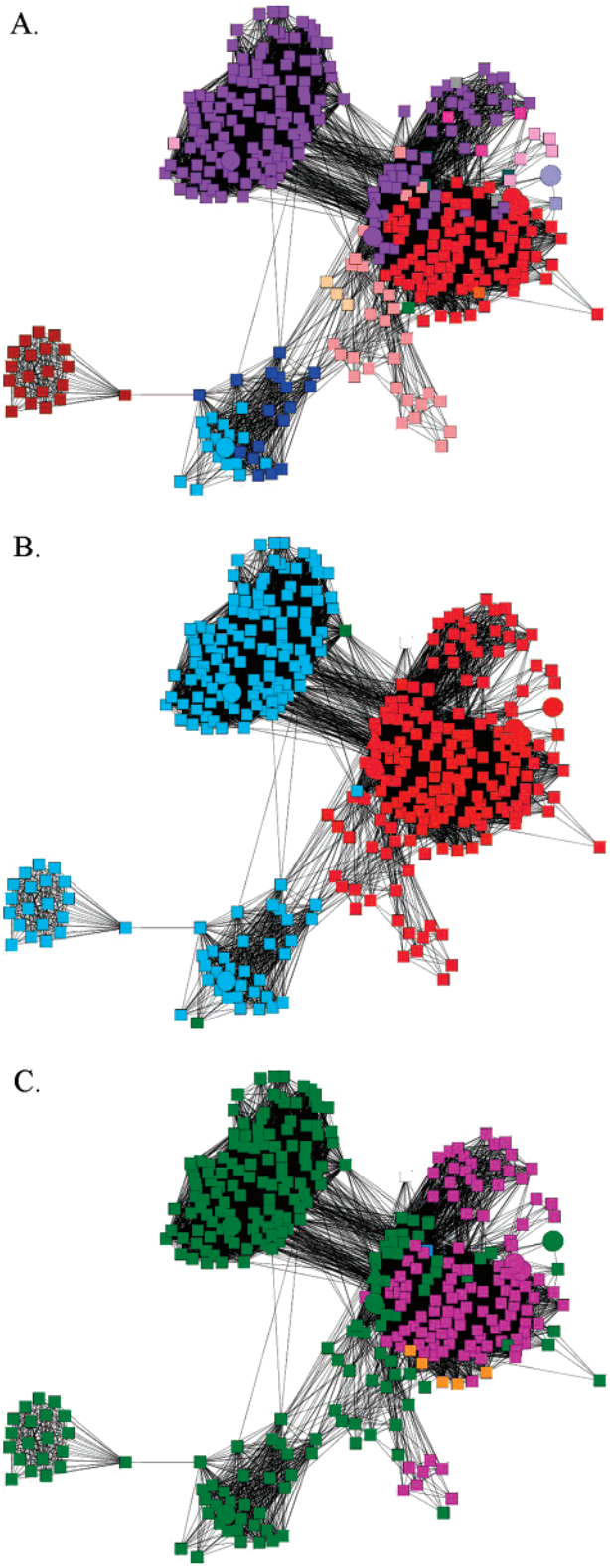


FIGURE 9: Cytoscape networks containing all members of the NagA-like sequence group. Nodes correspond to sequences and edges correspond to BLAST *e*-values. Uncharacterized sequences are shown as squares. Experimentally characterized and/or crystallized NagAs are shown as (larger) circles, and the sequence with experimentally determined AgaA activity is shown as a triangle. Networks are colored according to (A) lineage (colors correspond to those in Figure 8), (B) the amino acid types found at positions corresponding to the first two metal binding ligands in *B. subtilis* NagA (red, HxH; green, HxN; blue, QxN), (C) the residue type present at a position corresponding to His-143 in *E. coli* NagA (green, H; magenta, Q; orange, E; blue, M).

with either the QxN motif or the HxN motif (missing one or two of the α-metal binding ligands) has been shown to bind two metals, the *T. maritima* sequence (shown to bind only one metal) has the HxH motif. Thus there must be additional residues beyond the HxH motif that influence metal binding. One residue in particular, corresponding to His-143 in *E. coli* NagA, seems likely to influence metal binding. It is found in the active site of NagA, and is conserved in the group of sequences that cluster with enzymes known to bind only one metal. However, in the groups of sequences that cluster with the two-metal binding versions of NagA, it is conserved as either a glutamine or glutamic acid. Figure 9C shows the NagA-like sequence Cytoscape network, with sequences possessing a histidine at the position corresponding to His-143 in *E. coli* NagA colored green, those possessing a glutamine at this position colored magenta, and those possessing a glutamic acid at this position colored orange. A comparison of Figures 9B and 9C shows that all of the sequences missing the HxH motif (and thus, unable to bind more than one metal) have a histidine at the position corresponding to His-143. In addition, there are some sequences (including the one-metal-binding *T. maritima* NagA) that have the HxH motif, but also have a histidine at the position corresponding to His-143 from *E. coli*. This is consistent with the residue type at the position corresponding to His-143 of *E. coli* NagA influencing whether a sequence will bind one or two metals. However, due to the small number of NagA sequences with experimentally determined metal requirements, this hypothesis should be further tested. The Cytoscape networks given in Figures 9B and 9C may be useful for selecting test sequences for this purpose.

*Required Metal Ions for NagA from T. maritima.* The crystal structure of NagA from *T. maritima* contained a single Fe per active site (PDB ID: 1o12). The crystal structures shown in Figure 1 and the sequence alignment shown in Figure 2 demonstrate that this enzyme possesses the same metal binding residues as the NagA from *B. subtilis*, which contains two Fe atoms per active site. The absence of a metal ion in the $M_\alpha$-site of the *T. maritima* enzyme may have resulted in the loss of metal during the purification, or alternatively, this enzyme may not require a metal ion at this site. The metal titration studies presented in Figure 3 clearly show that the *T. maritima* enzyme requires only a single metal ion in the active site. This result is similar to the metal requirements for activation of NagA from *E. coli* (*21*).

*Structural Insights for Catalysis.* The characterization of the kinetic properties of the wild type NagA demonstrated that the most critical residue for the maintenance of catalytic prowess of this enzyme is Asp-273 (*21*). This residue is found at the end of β-strand 8, and the side chain carboxylate is hydrogen bonded to the water (or hydroxide) that is coordinated to the single metal ion in the active site. The homologous aspartate is of fundamental importance in all of the members of the amidohydrolase superfamily examined to date (*6*). It has been proposed that this residue functions as a general base to activate the hydrolytic water molecule via proton abstraction and then as a general acid during protonation of the leaving group amine. The postulated role of Asp-273 as a proton shuttle is further supported in the crystal structure of the Zn-containing wild type enzyme,

where Asp-273 interacts with the Zn-bound water molecule. Additional support for the critical role of Asp-273 is found in the structure of the D273N mutant which contains a phosphonamidate inhibitor in the active site. In this structure, Asn-273 is the closest group to the amide functional group of the inhibitor and is positioned to function in the protonation of the amino group of the departing glucosamine-6-phosphate. The reported inhibition constant of the inhibitor is 35 nM, and thus this compound is apparently a good mimic of the tetrahedral intermediate (*20*).

The anomeric hydroxyl group at C1 of the bound inhibitor is found in the α-configuration, which was also observed for the D-glucosamine product bound in the crystal structure of NagA from *B. subtilis* (*11*). This hydroxyl group is interacting with the side chain of His-251, and this residue is conserved in all of the NagA sequences identified to date. Another residue that contributes to the binding of the substrate is Arg-227. This residue forms an ion pair with the phosphate group of the substrate. Lys-139 is positioned more than 5 Å from any of the phosphate oxygens of the inhibitor. The magnitude of this distance is surprising, because the mutation of this residue results in a 25-fold increase in the Michaelis constant for the substrate (*21*). There are no residues interacting with the substrate that would help to discriminate between the two possible orientations of the hydroxyl at carbons 3 or 4. However, the hydroxyl group at carbon 3 is in position to hydrogen bond to one of the phosphonate oxygens of the inhibitor. This intramolecular interaction may be indicative of a structural or catalytic requirement of the substrate for NagA at carbon 3. The molecular interactions observed in the crystal structure of the bound inhibitor may preclude the utilization of sugars with an alternate stereochemistry at carbon 3, but not at carbon 4.

His-143, which originates from the loop at the end of β-strand 3, is absent in the structure of apo-NagA (PDB ID: 1ymy), but is found near the phosphonate group of the inhibitor. This residue may function in the active site by helping to polarize the carbonyl group of the amide bond during substrate hydrolysis in conjunction with the single divalent cation. Mutation of this residue reduces the value of $k_{cat}/K_m$ by up to 4 orders of magnitude (*21*). Similar interactions have been reported previously in the amidohydrolase superfamily for substrate activation by Tyr-137 in the reaction catalyzed by β-aspartyl dipeptidase (*35*).

## SUMMARY

Based on the metal titration studies and protein sequence comparisons, it is proposed that the structures of NagA from *B. subtilis*, *T. maritima*, and *E. coli* symbolize the evolution from the binuclear metal system present in *B. subtilis* and similar enzymes to the mononuclear metal systems observed in *E. coli* and in higher organisms such as *Homo sapiens*. It has been demonstrated that AgaA is very similar to NagA and that the only apparent difference is the location of the genes within the chromosome. We have verified that the two NagA enzymes from *E. coli* and *T. maritima* require only one metal for maximum activity. The HxH binding motif for the α-metal site used in NagA from *B. subtilis* NagA may be a vestige of evolution present in the NagA from *T. maritima*. The primary difference separating the single metal ion binding site found in NagA from *T. maritima* from the binuclear metal center found in NagA from *B. subtilis* appears to be the presence of a histidine residue that can function in the polarization of the substrate during bond cleavage.

## SUPPORTING INFORMATION AVAILABLE

Alignment of the amino acid sequences for NagA and AgaA. This material is available free of charge via the Internet at http://pubs.acs.org.

## REFERENCES


1. Uehara, T., and Park, J. T. (2002) Role of the murein precursor UDP-*N*-acetylmuramyl-L-Ala-gamma-D-Glu-meso-diaminopimelic acid-D-Ala-D-Ala in repression of beta-lactamase induction in cell division mutants, *J. Bacteriol. 184*, 4233−4239.
2. Uehara, T., and Park, J. T. (2003) Identification of MpaA, an amidase in *Escherichia coli* that hydrolyzes the gamma-D-glutamyl-meso-diaminopimelate bond in murein peptides, *J. Bacteriol. 185*, 679−682.
3. Uehara, T., and Park, J. T. (2004) The *N*-acetyl-D-glucosamine kinase of *Escherichia coli* and its role in murein recycling, *J. Bacteriol. 186*, 7273−7279.
4. Uehara, T., Suefuji, K., Valbuena, N., Meehan, B., Donegan, M., and Park, J. T. (2005) Recycling of the anhydro-*N*-acetylmuramic acid derived from cell wall murein involves a two-step conversion to *N*-acetylglucosamine-phosphate, *J. Bacteriol. 187*, 3643−3649.
5. Brinkkotter, A., Kloss, H., Alpert, C., and Lengeler, J. W. (2000) Pathways for the utilization of N-acetyl-galactosamine and galactosamine in *Escherichia coli*, *Mol. Microbiol. 37*, 125−135.
6. Seibert, C. M., and Raushel, F. M. (2005) Structural and catalytic diversity within the amidohydrolase superfamily, *Biochemistry 44*, 6383−6391.
7. Holm, L., and Sander, C. (1997) An evolutionary treasure: unification of a broad set of amidohydrolases related to urease, *Proteins 28*, 72−82.
8. Marti-Arbona, R., Fresquet, V., Thoden, J. B., Davis, M. L., Holden, H. M., and Raushel, F. M. (2005) Mechanism of the reaction catalyzed by isoaspartyl dipeptidase from *Escherichia coli*, *Biochemistry 44*, 7115−7124.
9. Benning, M. M., Shim, H., Raushel, F. M., and Holden, H. M. (2001) High resolution X-ray structures of different metal-substituted forms of phosphotriesterase from *Pseudomonas diminuta*, *Biochemistry 40*, 2712−2722.
10. Thoden, J. B., Phillips, G. N., Jr., Neal, T. M., Raushel, F. M., and Holden, H. M. (2001) Molecular structure of dihydroorotase: a paradigm for catalysis through the use of a binuclear metal center, *Biochemistry 40*, 6989−6997.
11. Vincent, F., Yates, D., Garman, E., Davies, G. J., and Brannigan, J. A. (2004) The three-dimensional structure of the *N*-acetylglucosamine-6-phosphate deacetylase, NagA, from *Bacillus subtilis*: a member of the urease superfamily, *J. Biol. Chem. 279*, 2809−2816.
12. Nitanai, Y., Satow, Y., Adachi, H., and Tsujimoto, M. (2002) Crystal structure of human renal dipeptidase involved in beta-lactam hydrolysis, *J. Mol. Biol. 321*, 177−184.
13. Liaw, S. H., Chen, S. J., Ko, T. P., Hsu, C. S., Chen, C. J., Wang, A. H., and Tsai, Y. C. (2003) Crystal structure of D-aminoacylase from *Alcaligenes faecalis* DA1. A novel subset of amidohydrolases and insights into the enzyme mechanism, *J. Biol. Chem. 278*, 4957−4962.
14. Marti-Arbona, R., Xu, C., Steele, S., Weeks, A., Kuty, G. F., Seibert, C. M., and Raushel, F. M. (2006) Annotating enzymes of unknown function: *N*-formimino-L-glutamate deiminase is a member of the amidohydrolase superfamily, *Biochemistry 45*, 1997−2005.
15. Ireton, G. C., McDermott, G., Black, M. E., and Stoddard, B. L. (2002) The structure of Escherichia coli cytosine deaminase, *J. Mol. Biol. 315*, 687−697.
16. Wilson, D. K., Rudolph, F. B., and Quiocho, F. A. (1991) Atomic structure of adenosine deaminase complexed with a transition-state analog: understanding catalysis and immunodeficiency mutations, *Science 252*, 1278−1284.
17. Williams, L., Nguyen, T., Li, Y., Porter, T. N., and Raushel, F. M. (2006) Uronate isomerase: a nonhydrolytic member of the

amidohydrolase superfamily with an ambivalent requirement for a divalent metal ion, *Biochemistry 45*, 7453−7462.
18. Ferreira, F. M., Mendoza-Hernandez, G., Castaneda-Bueno, M., Aparicio, R., Fischer, H., Calcagno, M. L., and Oliva, G. (2006) Structural analysis of *N*-acetylglucosamine-6-phosphate deacetylase apoenzyme from *Escherichia coli*, *J. Mol. Biol. 359*, 308−321.
19. Thoden, J. B., Marti-Arbona, R., Raushel, F. M., and Holden, H. M. (2003) High-resolution X-ray structure of isoaspartyl dipeptidase from *Escherichia coli*, *Biochemistry 42*, 4874−4882.
20. Xu, C., Hall, R., Cummings, J., and Raushel, F. M. (2006) Tight binding inhibitors of N-acyl amino sugar and *N*-acyl amino acid deacetylases, *J. Am. Chem. Soc. 128*, 4244−4245.
21. Hall, R. S., Xiang, D. F., Xu, C., and Raushel, F. M. (2007) *N*-Acetyl-D-glucosamine-6-phosphate deacetylase: substrate activation via a single divalent metal ion, *Biochemistry 46*, 7942−7952.
22. Pegg, S. C.-H., Brown, S., Ojha, S., Seffernick, J., Meng, E. C., Morris, J. H., Chang, P. J., Huang, C. C., Ferrin, T. E., and Babbitt, P. C. (2006) Leveraging enzyme structure-function relationships for functional inference and experimental design: the structure-function linkage database, *Biochemistry 45*, 2545−2555.
23. Edgar, R. C. (2004) MUSCLE: a multiple sequence alignment method with reduced time and space complexity *BMC Bioinformatics 5*, 113.
24. Li, W., Jaroszewski, L., and Godzik, A. (2002) Tolerating some redundancy significantly speeds up clustering of large protein databases *Bioinformatics 18*, 77−82.
25. Ronquist, F., and Huelsenbeck, J. P. (2003) MrBayes 3: Bayesian phylogenetic inference under mixed models, *Bioinformatics 19*, 1572−1574.
26. Otwinowski, Z., and Minor, W. (1997) Processing of X-ray diffraction data collected in oscillation mode, in *Methods in Enzymology* (Carter, C. W. J., Sweet, R. M., Abelson, J. N., and Simon, M. I., Eds.) pp 307−326, Academic Press, New York.
27. Terwilliger, T. C., and Berendzen, J. (1999) Automated MAD and MIR structure solution, *Acta Crystallogr., Sect. D: Biol. Crystallogr. 55*, 849−861.
28. Terwilliger, T. C. (2000) Maximum-likelihood density modification, *Acta Crystallogr., Sect. D: Biol. Crystallogr. 56*, 965−972.
29. Jones, A. T. (1985) Interactive computer graphics: FRODO, *Methods Enzymol. 115*, 157−171.
30. Brunger, A. T., Adams, P. D., Clore, G. M., DeLAno, W. L., Gros, P., Grosse-Kunstleve, R. W., Jiang, J. S., Kuszewski, J., Nilges, M., Pannu, N. S., Read, R. J., Rice, L. M., Simonson, T., and Warren, G. L. (1998) Crystallography & NMR system: A new software suite for macromolecular structure determination, *Acta Crystallogr., Sect. D: Biol. Crystallogr. 54*, 905−921.
31. McCoy, A. J., Grosse-Kunstleve, R. W., Storoni, L. C., and Read, R. J. (2005) Likelihood-enhanced fast translation functions, *Acta Crystallogr., Sect. D: Biol. Crystallogr. 61*, 458−464.
32. Lamzin, V. S., and Wilson, K. S. (1993) Automated refinement of protein models, *Acta Crystallogr., Sect. D: Biol. Crystallogr. 49*, 129−147.
33. Souza, J. M., Plumbridge, J. A., and Calcagno, M. L. (1997) *N*-acetylglucosamine-6-phosphate deacetylase from *Escherichia coli*: purification and molecular and kinetic characterization, *Arch. Biochem. Biophys. 340*, 338−346.
34. Bouma, C. L., and Roseman, S. (1996) Sugar transport by the marine chitinolytic bacterium *Vibrio furnissii*. Molecular cloning and analysis of the mannose/glucose permease, *J. Biol. Chem. 271*, 33468−33475.
35. Marti-Arbona, R., Thoden, J. B., Holden, H. M., and Raushel, F. M. (2005) Functional significance of Glu-77 and Tyr-137 within the active site of isoaspartyl dipeptidase, *Bioorg. Chem. 33*, 448−458.

BI700544C